Localized Surface Vibration and Acoustic Noise Emitted From Laboratory-Scale Transformer Cores Assembled From Grain-Oriented Electrical Steel

Anthony John Moses[1], Philip I. Anderson[1], and Teeraphon Phophongviwat[2]

[1]Wolfson Centre for Magnetics, Cardiff School of Engineering, Cardiff University, Cardiff, CF24 3AA, U.K.
[2]Department of Electrical Engineering, King Mongkut's Institute of Technology Ladkrabang, Bangkok 10520, Thailand

Magnetostriction of grain-oriented 3% SiFe sheets was measured prior to assembly into model transformer cores. Core vibration was measured using a laser scanning vibrometer and harmonic spectra of acoustic noise were evaluated from the microphone outputs. Explanations show why no correlation exists between vibration harmonics profiles and A-weighted acoustic noise spectra. High localized vibration did not cause high noise due to phase differences in surface vibrations, and it is shown that this is the main reason why the A-weighted noise of a three-phase core can be less than that of an equivalent single-phase core. Noise from cores assembled from low magnetostriction materials was not always lowest because of the variable effect of electromagnetic forces.

Index Terms— **Acoustic noise, electrical machine cores, electrical steels, magnetostriction, transformer cores, vibration.**

NOMENCLATURE

A_c	Limb cross-sectional area.
A_{cn}	Cross-sectional areas of clamping bolt.
B_c	Critical flux density.
B_g	Gap flux density B_p peak flux density.
B_n	Interlaminar flux density.
B_p	Peak flux density.
B_s	Saturation magnetization.
CGO	Conventional grain-oriented silicon steel.
EM	Electromagnetic.
GO	Grain-oriented silicon steel.
HGO	High-permeability grain-oriented silicon steel.
Hz	Hertz.
J	Bolt torque coefficient.
K	Environmental correction factor.
LDR	Domain-refined HGO.
L_{pA}	Corrected average A-weighted sound pressure level.
L_{pA0}	Average A-weighed sound pressure level.
L_{pi}	Sound pressure level.
L_{pAi}	A-weighed sound pressure level for each microphone.
L_{bgA}	Average A-weighted background noise pressure level.
MS	Magnetostriction.
MSL	Multistep lap.
N	Number of steps in an MSL joint.
N_{mic}	Number of microphones in the array.
N_s	Number of secondary turns.
RD	Rolling direction of electrical steel sheet.
SSL	Single-step lap.
T	Bolt clamping torque.
TD	Transverse direction.
V_{av}	Average value of induced voltage.
b	Instantaneous flux density.
e	Flux eccentricity ratio.
d_b	Bolt diameter.
f	Magnetizing frequency.
h	Height of segment.
l	Length of lamination.
p_i	Sound pressure.
p_{ref}	Reference pressure.
r	Circle radius.
rms	Root mean square.
s_{pp}	Peak-to-peak displacement.
ε	Strain.
σ_n	Surface clamping stress.
ω	Angular frequency ($\omega = 2\pi f$).
v_{rms}	Root mean square of surface velocity.
θ	Subtended angle.
δl_λ	Magnetostrictive strain.
δl_t	Total strain.
δl_M	Strain due to EM force.
$\mu\varepsilon$	Microstrain.

Manuscript received February 20, 2016; revised May 6, 2016; accepted June 6, 2016. Date of publication June 22, 2016; date of current version September 16, 2016. Corresponding author: A. J. Moses (e-mail: mosesaj@cf.ac.uk).

Color versions of one or more of the figures in this paper are available online at http://ieeexplore.ieee.org.

Digital Object Identifier 10.1109/TMAG.2016.2584004

I. INTRODUCTION

THE origins of acoustic noise emitted by a power transformer core and ways of controlling it have been studied for many decades. Today the demand for low-noise transformers is growing rapidly as more units are being sited in urban areas where size and weight rule out some established methods of noise limitation. The magnetic core vibration during the magnetizing process is the primary source of noise but the noise emitted from the fully assembled transformer is determined by its transmission through the cooling oil, etc., to the tank and how the tank then radiates the sound. The core vibration depends on many factors including the magnetostrictive properties of the magnetic core material, the design of corner joints in the stacked core, accurate positioning of lamination within the core, and also careful mechanical design of all components in the transformer to minimize resonance effects.

It is generally accepted that the two dominant sources of core noise are vibrations due to MS and EM forces but to date no method of estimating the contribution each makes to the noise of a given transformer core has been established. Contribution to knowledge and understanding of the mechanisms given in this paper will help in formulating suitable prediction methods.

Power transformer cores and most distribution transformer cores are assembled from laminations of electrical steel, grain-oriented 3% SiFe (GO). Commercial grades of GO can be grouped into three categories: conventional grain-oriented material (CGO), high-permeability material (HGO), and domain-refined HGO (LDR). MS of GO is very sensitive to mechanical stress which might be present in cores as a result of design or assembly [1]. However, no definite relationship between MS and core noise to quantify the benefit of using low-MS material has been established.

EM forces occur in laminated cores mainly where magnetic flux transfers between layers of laminations in core joints or jumps across air gaps between laminations at the joints. The small localized movement caused by these forces is a source of core vibration and noise. Today, multistep lap (MSL) joints [2] are widely used in stacked cores of distribution transformer primarily to reduce core losses, but a further benefit is that the corner joint flux distribution is more favorable, hence causing localized EM forces to be lower than those occurring in a single-step lap (SSL) joint, which in turn results in quieter cores.

It is difficult to determine what proportions of localized vibration of a core surface are due to MS or EM forces since at any position, one may dominate or they can be of the same order of magnitude. If the core flux density varies sinusoidally at 50 Hz, the vibration waveform will comprise a fundamental component at 100 Hz with a series of superimposed harmonics. Although these harmonics are mainly much lower in magnitude than the fundamental component, the noise they produce can be a major source of annoyance because of the frequency sensitivity of the human ear, e.g., the ear is around ten times more sensitive to a 1000 Hz component of noise than the one at 100 Hz.

Some important previous findings relevant to the investigation are given below together with some representative references.

1) Use of GO with low stress sensitivity of MS gives low core noise [1]–[5].
2) Vibrations due to localized MS and EM forces are the source of core noise [6]–[11].
3) Noise from MSL cores is generally lower than that of SSL assemblies [3]–[6], [10]–[14].
4) Core clamping methods have a major effect on noise [4], [8], [9], [12], [15].
5) MS velocity is a more relevant parameter to use than displacement when attempting to quantify the effect of MS on transformer noise [2], [4], [5], [13], [16].
6) The harmonics of MS and core vibration are at least as influential on core noise as the fundamental component [4], [6], [13], [17]–[19].
7) In three limb cores, the surface vibration is highest in the T-joints and the outer corners [5], [8], [20].

However, these findings are not quantified and sometimes concluded from a limited number of tests or observations. An important fact not widely appreciated in previous studies is that the out-of-plane surface vibration of the middle limb of a three-phase, three-limb core is 180° out of phase with that of the outer two limbs. This of course means that it is unlikely that a close correlation will exist between averaged peak vibration measurements, as commonly presented previously, and acoustic noise. In an investigation of load noise reported in [20], it is pointed out that this sort of phase difference results in a directed noise radiation. Earlier it was shown that the fundamental (first harmonic) out-of-plane vibration of the central limb of a three-phase core was 180° out of phase with the vibration of the outer limbs but its relevance to transformer noise was not discussed [21].

This paper reports on findings of a systematic study of noise and vibration of model transformer cores aimed at increasing our knowledge of the phenomena as well as expanding on some of the above findings. The emphasis of the work was to further our understanding of the fundamental mechanisms of core vibration and their influence on the noise. The use of smaller model cores enabled key parameters to be investigated while limiting the variation of other factors in the cores' design, manufacture, and operation. In the investigation, MS characteristics of single sheets of GO were measured before laminations were cut from the same batches of steel and assembled as transformer cores. The surface vibration distribution and acoustic noise outputs of the cores were systematically measured and analyzed.

II. Experimental Procedures

A. Magnetostriction Measurement

The peak-to-peak magnitude of the MS strain of GO, measured along its rolling direction (RD), is less than 1 $\mu\varepsilon$ (microstrain) and only varies by a small amount between the best and standard grades of steel in a stress-free state. However, when compressive stress is applied along the RD, MS increases rapidly to over 20 $\mu\varepsilon$ in a manner dependent on the steel's texture and surface coating. It is generally found that the use of grades of GO with low sensitivity to core building stresses leads to low noise cores [2], [3].

An established MS measurement system [22] was used as a model for an upgraded dedicated system [23] used in this investigation, in which longitudinal stress of up to ± 10 MPa could be applied during measurements to quantify the stress sensitivity of MS of strips of grades of steels chosen to assemble the studied cores. The peak-to-peak MS and mean vibration velocity of single strips of GO were measured at 50 Hz sinusoidal flux density. Commercial grades of 0.30 mm thick CGO, HGO, and LDR were selected. Fig. 1 shows representative MS characteristics measured along their RDs magnetized along the same direction at low and high flux densities. The uncertainty in the measurement of peak-to-peak MS was around $\pm 3.5\%$ of the recorded values.

The main points to note from the characteristics in Fig. 1 are the following.

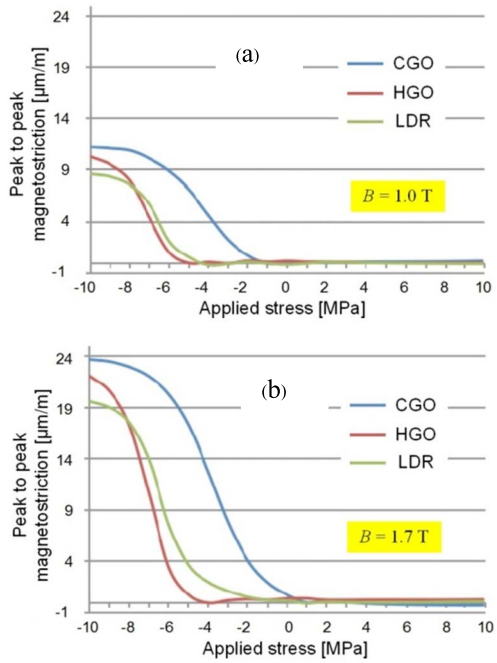

Fig. 1. Stress sensitivity of the peak-to-peak MS of strips of CGO, HGO, and LDR magnetized along their RDs at 50 Hz. (a) 1.0 T peak magnetization. (b) 1.7 T peak magnetization.

1) Under tension or zero stress, the magnitude of the MS of each material is less than $\pm 0.6\ \mu\varepsilon$ at both flux densities, implying that the MS-induced noise might be very low in a stress-free core and similar for each material.
2) As flux density is increased from 1.0 to 1.7 T, the critical compressive stress, at which MS begins to rise rapidly, falls by 30% (CGO), 60% (LDR), and 20% (HGO) from initial values of around −1.5, −4.0, and −5.0 MPa. This implies that the MS-induced noise in a moderately stressed LDR core will increase more with increasing flux density than in a similarly stressed HGO core.

In terms of MS improvement, the stress range over which HGO is advantageous over LDR is around −4.0 to −7.5 MPa at low flux density and between −2.0 and −7.5 MPa at high flux density. This demonstrates the possible desirability of quantifying and, if feasible, controlling the building stress in cores to optimize material selection. However, the potential noise reduction benefit of HGO over CGO is significant over the full compressive stress range.

It should be noted that the materials were selected to provide a wide range of magnetostrictive behavior and not to be representative of the individual grades, so no wider conclusions should be drawn from these initial results.

These observations of course only refer to MS-induced noise and, even then, rotational MS in the T-joints, which locally can be much larger than that occurring along the RD [24], and the harmonic content of the MS characteristic are not considered here.

B. Core Magnetization and Measurement System

Fig. 2 shows an overview of the transformer core testing system. A three-phase core was magnetized by a 15 kVA, three-phase autotransformer whose output voltages were

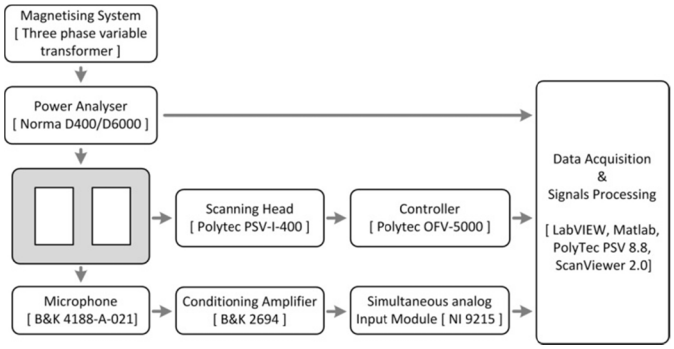

Fig. 2. Overview of the transformer core magnetizing method and the noise and vibration measurement process.

adjusted to produce balanced flux density in the three-phase, three-limb core under test (one phase of the autotransformer was used for energizing single-phase cores). The power analyzer was used to monitor induced voltages in 30-turn secondary windings wound around each limb. Prior to each noise or vibration measurement, the voltage induced in each coil was adjusted to produce peak flux density B_p given by

$$B_p = V_{\text{av}}/4.44 f N_s A_c \quad \text{T} \tag{1}$$

where V_{av} is the average value of the induced voltage, f is the magnetizing frequency, N_s is the number of secondary winding turns, and A_c is the cross-sectional area of the core limb. The limb flux densities were maintained sinusoidal to within a form factor tolerance of $1.11\% \pm 0.2\%$.

The transformer under test was placed vertically in a 2.0 m by 3.5 m by 2.2 m (height) hemi-anechoic acoustic chamber whose surfaces were covered with highly absorbent materials to avoid acoustic reflections.

A laser scanning vibrometer was used to measure the vibration profile of selected areas of the core surface. An array of microphones with matching amplifiers was used to obtain the sound pressure distribution at a fixed distance from the core surface. The measurement data were analyzed using LabVIEW and MATLAB. Fig. 3 shows a transformer under test with the vibrometer positioned above the core. The detailed methodologies are described in the following sections.

C. Vibration Measurement Methodology

A Polytec PSV-400 scanning vibrometer was used to measure the localized core vibration. Associated software provided graphics and animation in the form of 2-D color maps. The system was capable of measuring instantaneous surface velocity in the range of 0.01 μm/s to 10 m/s. Instantaneous and rms components of vibration velocity perpendicular to the plane of the laminations and the corresponding frequency spectra were averaged over 10 mm × 10 mm surface areas. The manufacturer's quoted maximum measurement error was less than $\pm 1.3\%$.

Mirrors, such as the one shown on the right-hand side of the core in Fig. 3, were used to scan three surfaces of the core under test without the need to move the vibrometer. A Polytec PSV 8.8 single-point vibrometer was used to compensate the output of the PSV-400 scanner for any spurious

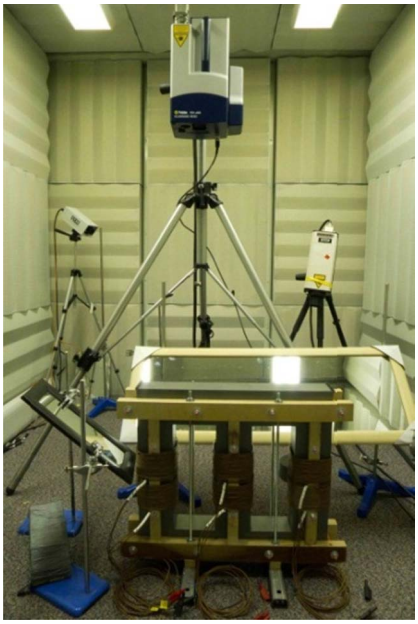

Fig. 3. Transformer core and vibrometer setup in the hemi-anechoic chamber.

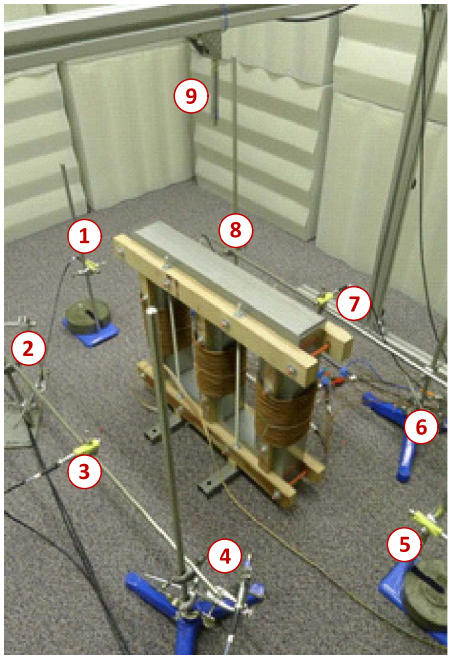

Fig. 4. Locations of microphones around and above a core under test in the acoustic chamber.

room vibrations. The average of three velocity readings was calculated at each measurement point during core testing.

D. Acoustic Noise Measurement

Conditions for measuring noise of commercial transformers as specified in IEC 60076-10 2001, Power transformers—Part 10: Determination of sound levels, were followed in this investigation. An array of eight B&K 4188-A-021 condenser microphones with frequency response range of 8 Hz to 12.5 kHz was positioned at half the height of the core with each microphone located 300 mm from the core surface as shown in Fig. 4. A virtual instrument was developed to determine the sound pressure and the sound pressure level detected by each microphone as well as the averaged A-weighted sound pressure and level (corrected for background noise). The sound detected by each microphone was measured simultaneously.

The measured sound pressure levels are independent of the environment and the distance of the microphones from the core, so the sound pressure and the sound pressure level recorded by each microphone could be analyzed in A-weighted true acoustic terms [25]. To do this, initially, the sound pressure p_i was calculated at each microphone position from its output voltage and sensitivity. The sound pressure level L_{pi} was calculated from

$$L_{\mathrm{pi}} = 20 \times \log_{10}\left(\frac{p_i}{p_{\mathrm{ref}}}\right) \ \mathrm{dB} \tag{2}$$

where the reference pressure p_{ref} is taken to be 20×10^{-6} Pa, which is approximately the threshold of human hearing at 1000 Hz. The A-weighted sound pressure level L_{pA0} averaged for all the microphones is given by

$$L_{\mathrm{pA0}} = 10 \times \log_{10}\left(\frac{1}{N_{\mathrm{mic}}}\sum_{i=1}^{N_{\mathrm{mic}}} 10^{\frac{L_{\mathrm{pAi}}}{10}}\right) \mathrm{dBA} \tag{3}$$

where L_{pAi} is the A-weighed sound pressure level for each microphone and $N_{\mathrm{mic}} = 9$ (the number of microphones). This equation was modified to incorporate the average A-weighted background noise pressure L_{bgA} and an environmental correction factor K which also corrected for the different radiating surfaces so that the noise output from three-phase and single-phase cores could be compared unambiguously [25]

$$L_{\mathrm{pA}} = 10 \times \log_{10}\left(10^{\frac{L_{\mathrm{pA0}}}{10}} - 10^{\frac{\mathrm{I}_{\mathrm{bgA}}}{10}}\right) - K \ \mathrm{dBA}. \tag{4}$$

The correction for background noise was applied after each live noise measurement. Its average value was only 22 dBA, so any error it might cause would be insignificant.

E. Core Design and Test Procedure

Cores were assembled from 100 mm wide laminations. Fig. 5 shows the overall dimensions and assembly of single- and three-phase cores. Approximately 250 layers of laminations were used. The total core masses of the three-phase and single-phase assemblies were 115 and 72 kg, respectively. Resonant vibration modes of this core geometry were calculated to confirm that they would not influence the investigation.

The cross-hatched areas are the regions over which localized vibrations were measured. Examples of the SSL and MSL joints used are shown in Fig. 6. The MSL assembly comprised four steps with an overlap length of 0.3 mm using one lamination per layer. Three laminations per layer were used in the SSL step cores with a 6 mm overlap. Fig. 6 shows the assembly of typical SSL and MSL corner joints.

Previous reports on the dependence of core noise on the number of laminations per step layer and the overlap length present conflicting conclusions. For example, [3] and [14] conclude that three- to four-step laps are the optimum number, whereas [12]–[15] state that three steps should be avoided.

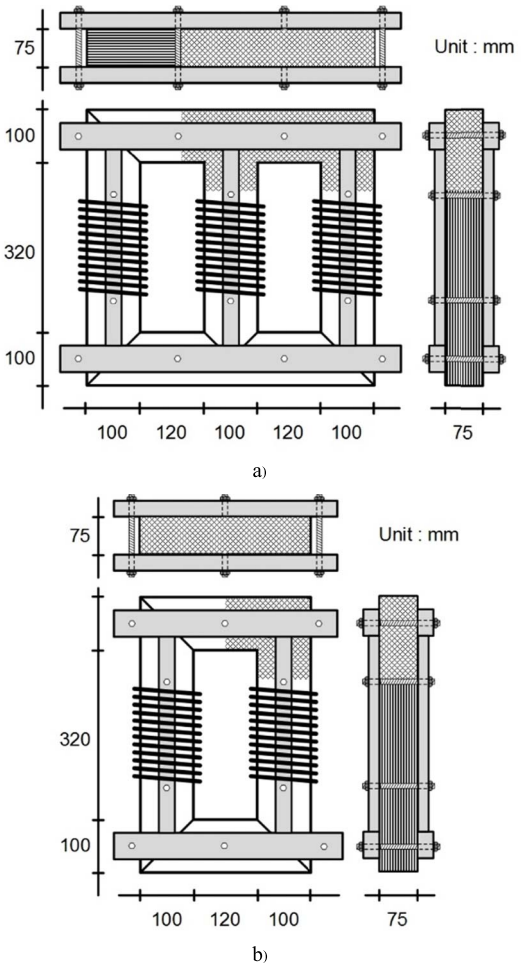

Fig. 5. Front views showing winding and clamping arrangement. (a) Three-phase core, 115 kg. (b) Single-phase core, 72 kg.

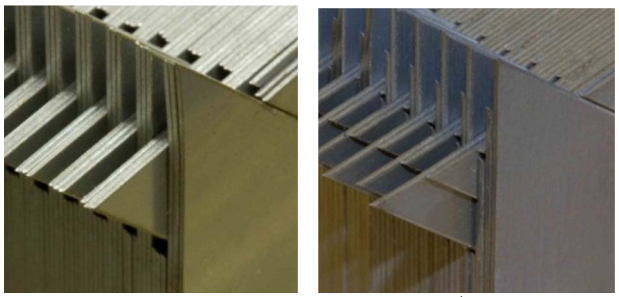

Fig. 6. Examples of corner joints. (a) Single step with three laminations per layer and 6 mm of length overlap shift. (b) Four-step MSL joint with one lamination per layer and 6 mm overlap length (these are not the values used in the investigation but are included for illustration).

Also [3] and [14] report that using two or three laminations per layer instead of one has a marginal effect on noise whereas [13] and [26] say that this increases noise. Early comprehensive work on single-phase cores showed that the noise increases monotonically with increasing overlap length in SSL joints [27], whereas [12] and [14] state that overlap length of 2 mm should be avoided. The apparently conflicting results in these examples are most likely due to the fact that many variables associated with core design, material selection, magnetization level, etc., which influence the variation of noise with joint design, are not likely to be the same in each investigation, so differing conclusions are not surprising. Hence, the corner joint configurations chosen for this investigation were based on practicality and experience taking into account the previous findings.

As mentioned in Section I, the core clamping method has a large influence on noise. In this investigation, 50 mm by 30 mm wooden clamping plates were positioned on either side of each yoke and 30 mm $\times$ 20 mm plates on each limb as shown in Fig. 5. The clamping plates are secured by 8 mm-diameter-reinforced plastic bolts (14 in all for the three-phase core), each tightened to a torque of 4.0 N $\cdot$ m for the main tests. The average out-of-plane component of surface clamping stress σ_n depends on the position and number of core clamps; in these configurations, it is calculated from [28]

$$\sigma_n = T/Jd_bA_{\text{cn}} \text{ Pa} \tag{5}$$

where T is the bolt torque, J is the torque coefficient (assumed as 0.45 for such steel bolts), d_b is the bolt diameter, and A_{cn} is the cross-sectional area to which the bolt force is applied. The stress on each layer of laminations varies with depth into the core and drops on moving away from each bolt. In this case, $\sigma_n \approx 0.08$ T. Hence, if each bolt is tightened to 4.0 N $\cdot$ m, the average normal stress at the core surface is 0.33 MPa.

F. Measurement of Localized Flux Density in a Core

Because of GO's large grains and high in-plane anisotropy and the complex 3-D flux paths, it has so far been impossible to accurately predict localized components of flux density in the joints using computational EM solvers, so time-consuming experimental methods are still necessary. Laminations from one layer of a core were selected for hosting search coils for localized flux density measurements. An array of 10 mm long, single-turn 0.19 mm diameter enamel-covered copper wire search coils was wound through 0.5 mm diameter holes drilled in the laminations.

The laminations were assembled in the central region of a three-phase, MSL CGO core which was magnetized as described in Section III-A. The magnitude and phase of the emfs induced in the pairs of orthogonal coils were measured, and the instantaneous magnitude and direction of the localized flux at each point were calculated using a well-established technique [29].

III. Preliminary Measurements

A. Reproducibility of Measurements

Since only small changes in core characteristics might occur due to controlled changes in joint geometry, clamping stress, core material, etc., the reproducibility and random building variability of the noise measurements were first determined. The noise output of a single-phase MSL was measured using the procedure outlined in Section II and the measurement repeated three times after re-magnetizing to nominal flux densities of 1.5–1.8 T. The core was next dismantled and reassembled and the sequence of measurements repeated. The repeatability of measurements on the assembled core was within $\pm$0.5 dBA whereas the variation after re-assembly

increased from around 1.0 dBA at 1.5 T to 4.0 dBA at 1.7 and 1.8 T. Build variations of ±6 dBA, and even higher for individual harmonics, have been reported for MSL cores [14], [15] so the careful building practice adopted here made the variations as low as practically achievable.

To determine the variation in noise of identical transformers assembled from laminations from the same batches of materials, pairs of SSL and MSL three-phase cores were assembled and tested. Four cores of each material, two with SSL joints and the other two with MSL joints, were magnetized between 1.5 and 1.8 T with bolt torques of 4.0 N · m.

A small difference of 1.5 dBA on average between the noise of nominally identical transformers in the other pairs can be attributed to core build variations. The noise of the MSL cores was on average 4 dBA lower than that of equivalent SSL cores. The noise of the CGO cores was consistently higher than that of cores assembled from the other materials presumably due to their poorer stress sensitivity.

B. Variation Due to Clamping

In order to assess the effect of the clamping method, a three-phase, MSL core assembled from CGO was clamped tightly for confirming that the limbs were flexing rigidly at bolt torques of 2.0–6.0 N · m. The A-weighted sound pressure level emitted from the core was measured at three microphone locations. It was found that the noise did not vary with clamping pressure any more than could be attributed to normal build variations. Previous reports show that noise increases by around 3 dBA as clamping torque increases from 15 to 30 N · m [26] but [4] reported an optimum clamping stress in the range 0.075–0.10 MPa according to joint design and operating flux density. Unsurprisingly, this is not much less than the 0.33 MPa (4.0 N·m bolt torque) value found here, which itself is a maximum localized value obtained from (5), so it is far lower than the average value throughout the core.

The dependence of surface vibration on clamping stress was investigated using the laser scanning vibrometer. Fig. 7 shows the surface vibration patterns observed on the front surface of a CGO core magnetized at 1.7 T under different clamping torques. The figure shows the localized, out-of-plane rms component of velocity over the surface area depicted by the hatched areas in Fig. 5, i.e., over lamination surfaces in the upper right-hand portion of the core including regions in the T-joint and corner joint not obstructed by the clamps. The anticipated highest vibration velocity occurs in regions of the T-joint and central limb as well as the outside corner joint at all three clamping pressures. There is high lamination flapping in the outer joint at 2.0 N·m and a significant increase in vibration in the central limb at high clamping stress.

The vibration amplitude appears to increase with increasing clamping stress although the acoustic noise dropped at an intermediate clamping stress. It is shown in Section IV that a direct correlation between rms surface velocity and noise output should not be expected.

Since a clamping torque of 4.0 N · m has the least effect on noise, it was decided to use this setting throughout the investigation.

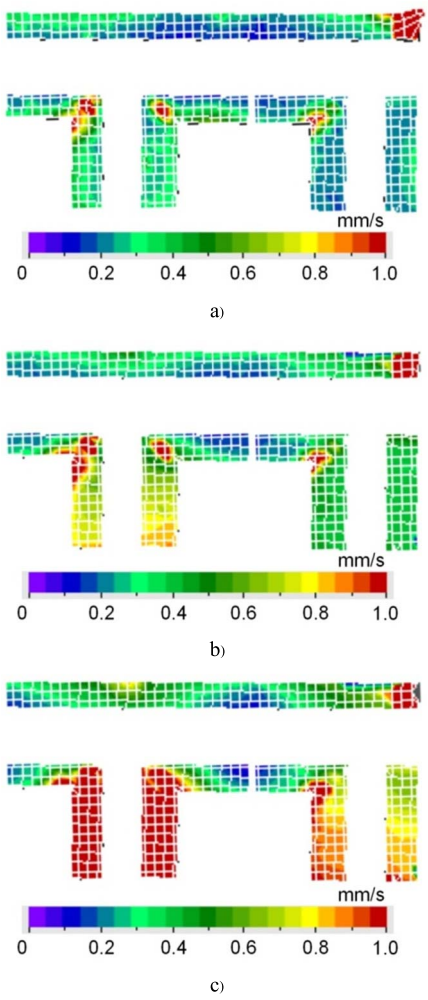

Fig. 7. Distribution of rms component of out-of-plane vibration measured on a CGO MSL core at 1.7 T with clamping torques of (a) 2 N · m, (b) 4 N · m, and (c) 6 N · m.

In order to fully understand the vibrometer measurements, it is useful to develop the basic relationship between rms velocity of a surface and the corresponding displacement. Suppose a lamination is vibrating sinusoidally in time at frequency ω, the driving force being magnetostrictive or EM. If one end of the lamination is fixed and it is vibrating in its plane, then the peak-to-peak displacement of the other end during each cycle of magnetization is given simply by

$$s_{\mathrm{pp}} = \sqrt{2} v_{\mathrm{rms}}/\omega \quad \mathrm{m} \tag{6}$$

where v_{rms} is the rms velocity. If we take an example of a typical measured velocity of 1.0 mm/s and frequency of 100 Hz, typical of the measurements being presented in this paper, then $s_{\mathrm{pp}} = 2.2\ \mu$m. If this occurs on a 550 mm long yoke lamination, then the peak-to-peak strain is 2 $\mu\varepsilon$. In practice, the velocity will change sinusoidally in time but this example shows that the magnitude of the associated displacement is compatible with that of MS in GO.

C. Noise Distribution Pattern Around a Core

Noise output of each core was normally calculated as described in Section II-D by averaging the outputs of the

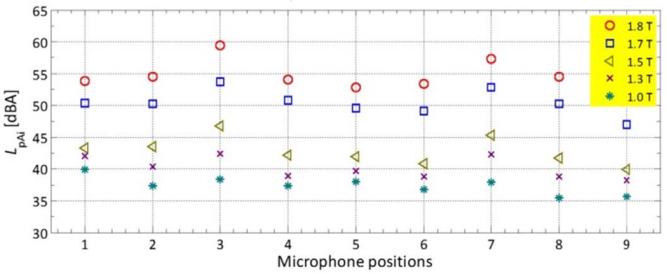

Fig. 8. Variation of averaged (three trials) A-weighted sound pressure level from a microphone placed on the prescribed contour (positions 1 to 8) of and above (position 9) the three-phase MSL CGO core at flux densities of 1.0–1.8 T, 50 Hz.

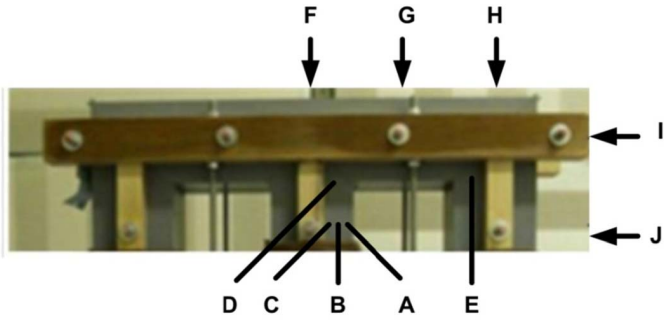

Fig. 9. Positions at which localized vibration was measured on the surface of the three-phase MSL CGO core.

microphones at locations shown in Fig. 4 using the IEC guidelines. However, initially it was decided to measure the variation of noise around a core from the outputs of the individual microphones. A CGO three-phase MSL core was placed in the chamber and magnetized at 1.0–1.8 T. The A-weighted noise output from each microphone was recorded separately to produce the distribution shown in Fig. 8. At high flux density, the noise detected by the microphones opposite to the two sides of the central limb is 4–5 dBA higher than that measured at any other position, but at 1.0 T, it was only marginally higher. The noise detected above the core (position 9) was generally lower than that detected by microphones positioned around the core. The higher than average noise level adjacent to the central limb is possibly due to larger vibration in that limb as will be seen later.

Examining the noise detected by the individual microphones in this way can help identify regions where high vibration occurs. Unless stated otherwise, the noise measurements presented in the later sections are all the average of the nine microphone readings which was found to reduce the measurement uncertainty, due primarily to the relative positioning of the microphones and core, to less than ±2%.

IV. Experimental Measurements and Analysis

A. Core Front Surface Noise and Localized Vibration

The harmonic spectrum of the vibration at the selected points on the core surface shown in Fig. 9 was investigated. At points A, B, and C, the core was expected to be subjected mainly to alternating flux density along the RD of the laminations. At D, within the T-joint region, rotational magnetization occurs and out of RD components of flux [35] could occur at E, in the corner region. Any differences in vibration measured at A, B, and C could be attributable to nonuniform clamping stress with position C being farthest from the most highly stressed region under the clamp or localized flux distortion but no differences were actually found.

TABLE I
Variation of rms Values of Harmonics of Surface Velocity [μm/s] at Locations on the Surface of the CGO MSL Core Magnetized at 1.0, 1.5, and 1.7 T, 50 Hz

f [Hz]	A/B/C (centre limb)			D (T-joint)			E (corners)		
	1.0 T	1.5 T	1.7 T	1.0 T	1.5 T	1.7 T	1.0 T	1.5 T	1.7 T
100	313	747	1027	351	1272	1006	348	276	957
200	11	36	153	25	849	1254	111	378	1015
300	4	10	89	32	125	682	18	334	620
400	3	19	92	10	349	294	11	96	165
500	2	17	36	2	110	442	13	142	205
600	1	7	59	3	68	271	8	92	150

Table I shows the results when magnetized at 1.0–1.7 T. No significant difference between the vibration characteristics at A/B/C was apparent, so the values are averaged in the table. It is noticeable that the vibration at the locations outside the corners is dominated by the fundamental (100 Hz). At points D and E, the higher harmonics are significant, undoubtedly related to complex localized magnetization or rotational MS [24] in the joint regions.

Localized flux density measurements were made to help estimate the importance of rotational MS in this case. The laminations on which localized search coils were mounted as described in Section II-F were inserted into the central region of the core. The localized flux density was measured while the core was magnetized sinusoidally at 1.7 T. In central regions of the yokes and the limbs the localized flux contained up to 9.4% third harmonic components distributed in a random manner as expected [30]. At the outer corner joints, the harmonic content increased to 38.1% but the transverse component of flux did not exceed 0.13 T when the peak flux density in the RD was 1.7 T.

An important finding supporting early work [31] is that at no point in the T-joint did the flux eccentricity ratio (e = peak value of TD component/peak value of RD component) exceed 0.2. This was not surprising since it has been claimed that rotational flux in a T-joint is highly elliptical and pure rotational flux ($e = 1.0$) does not normally occur in such transformer cores [32]. This has important implications on the widely promoted view that rotational magnetostriction (i.e., due to pure rotational flux) is a major cause of core vibration [10].

The frequency spectrum of the sound pressure at the front surface of the same CGO MSL core was measured and the results are summarized in Fig. 10. The 100 Hz (fundamental) component only dominates at low flux density, whereas the second and third harmonics become prominent at higher flux densities.

The average sound pressure (Pa) from a measurement system in the time domain is converted to sound

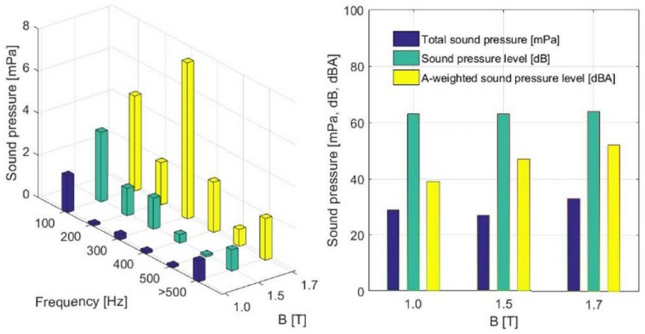

Fig. 10. Harmonics of sound pressure [mPa] emitted from the front surface of the three-phase CGO core at 1.0, 1.5, and 1.7 T, 50 Hz (detected by microphone 3).

pressure level (dB) in the frequency domain using (2) and then transformed to the A-weighted sound pressure level (dBA). It can be noted that although the sound pressure (and proportional sound pressure level) is lower at 1.5 T than at 1.0 T, the corresponding A-weighted value is higher at 1.5 T. This demonstrates the impact of allowing for the response of the human ear by A-weighting. However, there is no correlation between the distribution of vibration and noise harmonics in Table III associated with different regions of the core.

The equivalent components of out-of-plane rms vibration patterns on the front surface of the core magnetized at 1.0–1.7 T are shown in Fig. 11. No correlation with the noise measurement data presented in Fig. 10 is apparent but the average corner and central limb vibration is two to over four times higher than that in the yoke, the factor increasing with increasing flux density, confirming that these regions are the source of highest vibration in three-phase cores. The rms velocities averaged over the corner regions, the central limb, and T-joints are shown on the contour distributions to help quantify the effect.

Although A-weighted sound power level is gaining acceptance as a reference quantity for quantification and comparison of noise generated from transformer cores, it is not suitable for investigating the relationship between noise and vibration because the A-weighting scale is applied to the sound pressure signal. Sound pressure and the vibration signal in the frequency domain are the most appropriate parameters for studying the relationship between transformer core noise and vibration.

B. Core Side and Top Surface Noise and Localized Vibration

Core noise and vibration were measured with respect to side and top surfaces of the CGO MSL core using the same approach as presented in the previous section. Fig. 12 shows the harmonic spectrum of the velocity recorded at the positions indicated in Fig. 10 on the top (points F, G, and H) and side (points I and J) surfaces of the core. At 1.0 T, very little harmonic distortion was observed. Even at higher flux densities, the fundamental component and harmonics are far lower than those found on the front surface. The results show that the rms velocity components on the side surface are even lower than those on the top surface. Only a small

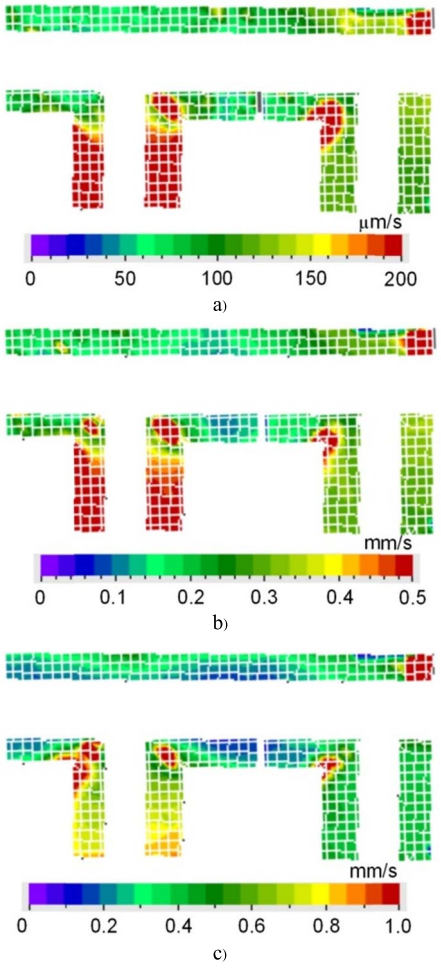

Fig. 11. rms vibration velocity distribution on the front surface of the CGO MSL core at (a) 1.0 T, (b) 1.5 T, and (c) 1.7 T.

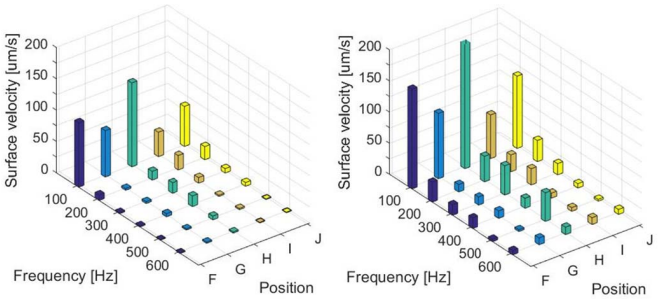

Fig. 12. Variation of rms values of harmonics of surface velocity (μm/s) at locations on the front and side surfaces of the CGO MSL three-phase core magnetized at 1.0–1.7 T, 50 Hz.

number of measurement points are considered here, but they are representative of the low harmonic components in the vibration of the side and top surfaces.

Table II shows corresponding frequency spectra of the sound pressure associated with the side and top surfaces of the core from microphones 1 and 9, respectively. Obviously, they are not directly related to the localized rms velocity data just presented since the microphones are sensitive to envelopes of sound emitted from large regions of the core whereas the vibration measurements are spot readings.

TABLE II
HARMONICS OF SOUND PRESSURE [mPa] EMITTED FROM SIDE (POSITION 1) AND TOP (POSITION 9) SURFACE OF THE THREE-PHASE CGO CORE MAGNETIZED AT 1.0, 1.5, AND 1.7 T

	Side surface			Top surface		
	1.0 T	1.5 T	1.7 T	1.0 T	1.5 T	1.7 T
100 Hz	0.65	1.1	1.5	0.4	0.55	0.5
200 Hz	0.48	2.5	5.5	0.4	0.95	0.6
300 Hz	0	0.7	4.0	0.2	0.3	0.9
400 Hz		0.3	1.6	0.11	0.2	0.3
500 Hz		0.2	0.9		0.1	0.9
500-4000 Hz	< 0.15	< 0.25	< 0.6	0.15	0.25	0.5
Total sound pressure [mPa]	34	32	36	26	23	28
Sound pressure level [dB]	65	64	65	62	61	63
A-weighted sound pressure level [dBA]	40	43	49	36	39	46

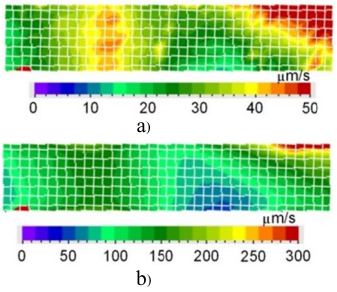

Fig. 13. Distribution of in-plane component of rms velocity (μm/s) on the top surface of the CGO, MSL core at (a) 1.0 T and (b) 1.7 T.

The sound pressure associated with the side surface is higher than that of the top surface although significantly less than that of the front surface. The harmonic components of both increase with flux density possibly due to the increasing prominence of MS harmonics [32], although generally they are lower than the equivalent noise harmonics shown in Table IV associated with the front surface of the core.

The 100 Hz components measured at the side and edge of the core were consistently around 65% and 83%, respectively, lower than that on the front surface over the full flux density range but there is no obvious trend with the higher harmonics. The 200 Hz and 300 Hz harmonic components measured adjacent to all three surfaces dominate at 1.5 and 1.7 T, but the varying harmonic distributions are not reflected in the noise characteristics detected by the individual microphones as shown in Fig. 9.

The vibration patterns over the top and side core surfaces are presented in Figs. 13 and 14, respectively. It can be seen from Fig. 13 that the highest vibration velocity at any point on the top surface is around 50 and 300 μm/s at 1.0 and 1.7 T, respectively, compared with equivalent values of 200 and 1000 μm/s on the front face of the core as shown in Fig. 11.

Also the vibration velocity of the top surface above the central limb and outer limb is two to three times higher than that at the center of the yoke region. This can be attributed

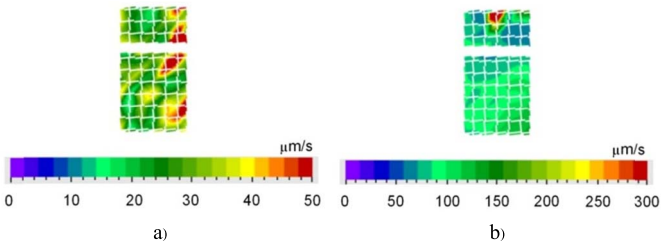

Fig. 14. Distribution of in- plane component of rms velocity (μm/s) on the side surface of the CGO, MSL core at (a) 1.0 T and (b) 1.7 T.

TABLE III
COMPARISON OF SOUND PARAMETERS MEASURED BY MICROPHONES ADJACENT TO FRONT, SIDE, AND TOP SURFACES OF THE CGO MSL CORE

	Front		Top		Side		Average	
	1.0 T	1.7 T	1.0 T	1.7 T	1.0 T	1.7 T	1.0 T	1.7 T
Sound pressure [mPa]	29	33	26	28	34	36	29.5	34.3
Sound pressure level [dB]	63	64	62	63	65	65	63.4	64.3
A-weighted sound pressure level [dBA]	39	52	36	46	40	49	38.8	49.8

to the extension of the limbs tending to bend the yoke in the normal direction (out of plane) to a small extent; whether the mechanism is simply an opening and closing of the joints or actual physical bending of the yoke laminations in their stiff transverse direction is debatable.

In an ideal case where no out-of-plane vibration occurs, the measured yoke top surface velocity above the limbs should be the same as the in-plane vibration of the limb laminations themselves. At 1.7 T, the top surface vibration velocity is around 130 μm/s above the central limb inferring a longitudinal strain of 3 $\mu\varepsilon$ in the central limb, which could be caused by a combination of EM-induced strain originating in the T-joints and a magnetostrictive strain if the laminations were stressed to around 1–2 MPa in the case of the CGO material.

The surface vibration velocity distribution over the upper 170 μm/s length of a side limb is shown in Fig. 14 (the horizontal strip where no data is shown is obscured by an external tie bolt). The average rms vibration velocity over the measured area on the side of the core at 1.0 and 1.7 T is 38 and 100 μm/s compared with 40 and 130 μm/s on the top surface and 150 and 600 μm/s on the front surface. These are arbitrary measurement areas but the results do help visualize the vibration pattern over the full core. The maximum rms vibration velocity at both flux densities is similar in magnitude to the maximum on the top surface. The non-symmetry of the distributions on the top and side faces might be due to the inherent geometrical non-symmetry of the step lap T-joint. The sound parameters measured at the microphone positions adjacent to the front, top, and side surfaces are summarized in Table III. The highest sound pressure (mPa) and corresponding pressure level (dB) are from the side surface where the surface vibration velocity is relatively low, certainly

compared with the front face. Although the surface velocity of regions of the front face is very high, the sound pressure and the A-weighted noise are low. The amplitude of the average rms vibration velocity of the top surface is higher than that of the side surface but the sound pressure is lower as shown in Table III. This is the effect of time phase difference between vibrations at different parts of the top surface highlighted in the next section. It should be emphasized that the values in Table III are only included to help clarify the complex relationships between localized vibration and sound profiles, and they do not represent global conditions over complete core surfaces. Hence, the average values have no physical meaning but help show overall trends.

C. Variation of Time Phase of Surface Vibration in the Three-Phase Core

The results presented in Section III-B show that the front surface of the CGO core exhibited the highest out-of-plane vibration velocity and the 100 Hz component dominates whereas the associated acoustic noise was unexpectedly low. Figs. 11, 13, and 14 show the rms velocity distribution on the core surface, which is directly related to localized displacement but does not show information about the variation from point to point in time phase during the magnetizing cycle. In this section, the effect of the 120° phase difference between the flux densities in the three limbs of the three-phase core on the magnetostrictive strain and the variation of the *instantaneous* value of the 100 Hz component of out-of-plane velocity throughout a magnetizing cycle is considered.

Fig. 15 shows the theoretical variation of instantaneous magnetic flux density at four instants in a magnetizing cycle assuming that the fluxes in each phase vary sinusoidally and are 120° out of phase with each other. Making use of the symmetry, only half of the core is shown. The reference time $\omega t = 0°$ is defined as the instant in the magnetizing cycle when the flux density in the central limb B is zero. The light gray vectors indicate the positive reference direction and the magnitude of the peak flux density. The bolder vectors represent, to the same scale, the instantaneous magnitudes and directions of b, the instantaneous flux density.

Fig. 15 also gives an indication of the longitudinal magnetostrictive distortion in the laminations obtained using a MATLAB model developed to visualize the deformation assuming ideal uniform flux distribution shown. It does not take rotational magnetization and ac magnetization out of RD or EM forces into account.

At $\omega t = 0°$, the flux density in limb B is zero while it is 0.866 B_p in limb A and 0.866 B_p in the opposite direction in limb C, where B_p is the peak value of the nominal flux density (the direction of the flux does not affect the amplitude of MS). At this instant in time, the dimension of limb B is unchanged because its flux density is zero but the yoke is deformed as it carries the circulating flux. If we assume that the MS is approximately proportional to b^2 [32], then the strain in each outer limb and the yokes at this instant is 0.866^2 or 75% of the maximum MS. This creates the possibility of equally high magnetostrictive strain in the four outer corners together with lower strain at the T-joints.

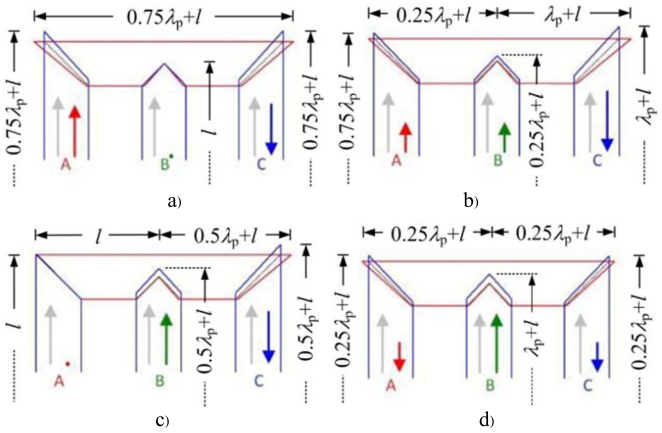

Fig. 15. Representations of magnitude and direction of instantaneous flux density and simulated magnetostrictive distortion at (a) $\omega t = 0°$ and 180°, (b) $\omega t = 30°$, (c) $\omega t = 60°$, and (d) $\omega t = 90°$.

Using a similar approach, it can be deduced that at $\omega t = 30°$ the strain profile shows high values at diagonally opposite corners tending to bend the core and in the T-joint region at the same time tending to push the yokes apart. It can be seen that at $\omega t = 60°$ there is no strain in limb A, so the core is non-symmetrically strained, and when $\omega t = 90°$, all corners are again symmetrically strained.

The deformation patterns indicated in Fig. 15 are greatly exaggerated to illustrate the effect. In practice, the maximum longitudinal magnetostrictive strain in mechanically stressed GO is of the order of 20 $\mu\varepsilon$, which equates to extension of around 10 μm in the core laminations here, which in turn is sufficient to cause joint noise or lamination bending. This superficial overview of in-plane magnetostrictive strain variation during a cycle includes several approximations and assumptions which make any quantified values of the resulting surface velocity or displacement very uncertain, but it is helpful in trying to interpret the complex variation of instantaneous out-of-plane vibration measurements presented in Fig. 16. It is possible that core distortion caused by this phenomenon could interact with similar distortion predicted due to core resonance, see [17], [33].

It is most likely that the relationship between the out-of-plane vibration of a core and the in-plane magnetostriction is dependent on the mechnaical stiffness and rigiditiy of the corner joints, which themselves can vary according to the consistency of assembly from core to core. Further study is necessary to verify that this is the main cause and to quantify it.

Fig. 16 shows the measured instantaneous out-of-plane surface velocity of the MSL CGO core, magnetized at 1.7 T, at the same instances in time as shown diagrammatically in Fig. 15. The surfaces where no velocity distribution pattern is shown are obscured by magnetizing coils or clamps.

At $\omega t = 0°$, the flux density in the middle limb is zero; the MS of the laminations in the middle limb is also zero but the limbs are possibly subjected to forces at their ends due to the MS in the yoke laminations, which is a possible explanation for the low small vibration in the middle limb shown in Fig. 15 at $\omega t = 0°$ or $\omega t = 180°$. However, at

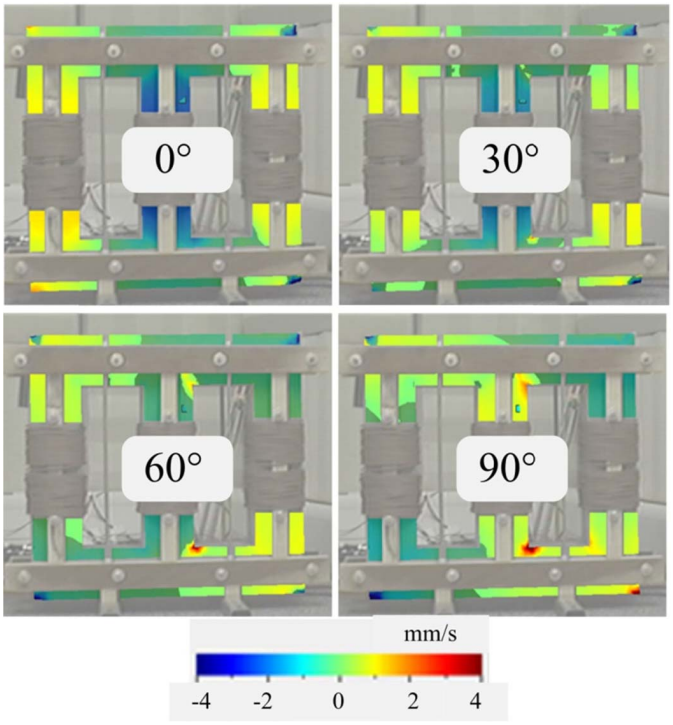

Fig. 16. Measured instantaneous velocity contour on the front surface of the CGO MSL core with clamping pressure of 0.33 MPa at $\omega t = 0°$ (180°), 30°, 60°, 90° at $B_p = 1.7$ T.

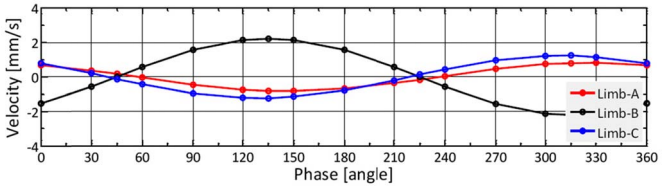

Fig. 17. Comparison of measured variation of instantaneous fundamental velocity (100 Hz) at the center and half height on each limb during one cycle of magnetization between the central limb (Limb-B) and outer limbs (Limb-A and Limb-C) at 1.5 T, 50 Hz.

the same instant in time, the highest vibration is close to one pair of diagonally opposite corners, which cannot be explained from the magnetostrictive strain postulated in Fig. 15.

The model in Fig. 15 only shows the relationship between the magnetizing signal and MS, but Fig. 16 shows the effect of both MS and magnetic forces on the core. Because vibration displacement is not only magnetostrictive, zero core vibration velocity occurs when core vibration displacement is zero but not necessarily when MS is zero.

At $\omega t = 30°$, the velocity of the central limb is highest although the MS of limb C is highest at this time. At $\omega t = 90°$, the vibration of the middle limb has risen to its maximum amplitude. Although no experimental observations could be made at the center of the middle limb, it can be assumed from the trend that the highest vibration of the middle limb is at its center with amplitude approximately twice that of the outer limbs. This is seen in Fig. 17, which compares the time phase of the bending motion of the three limbs. It can be noted from Fig. 11 that at 1.5 T the average rms velocity

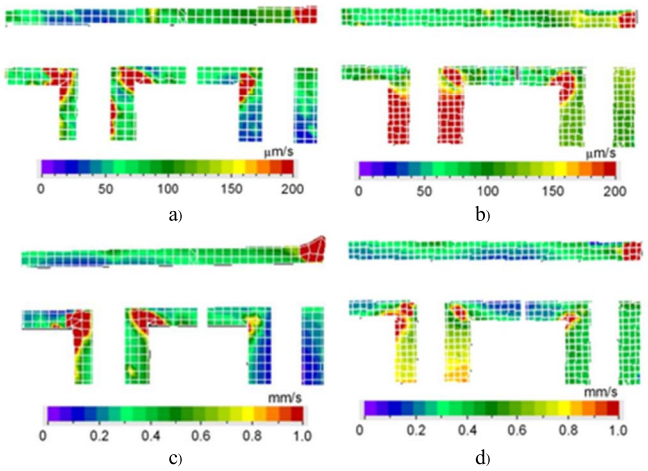

Fig. 18. Distribution of rms value of localized out-of-plane velocity of the front surface of CGO cores. (a) SSL, 1.0 T. (b) MSL, 1.0 T. (c) SSL, 1.7 T. (d) MSL, 1.7 T.

in the central limb is around 0.55 mm/s and in limb C it is around 0.30 mm/s, implying peak values of around 0.80 and 0.40 mm/s, respectively, whereas the respective peak values in Fig. 17 are 2.0 and 1.0 mm/s, respectively. This difference occurs because the rms value of the total vibration is considered in Fig. 11 whereas the peak value of the 100 Hz component is presented in Fig. 16. This clearly shows that the vibration velocity of the outer two limbs is around 180° out of phase with that of the central limb. Hence, the acoustic waves generated at the surface of the central limb, which is vibrating at double the amplitude of the outer limbs, will be cancelled out to a large extent by those generated by the motion of the outer two limbs, the amount of cancellation being proportional to the cosine of the phase difference between the waves [25], which in this case (cos 180°) results in optimum cancellation in the three limbs at 1.5 T.

D. Comparison of Surface Vibration Modes and Harmonics in SSL and MSL Cores

Surface vibration studies were made on CGO three-phase SSL and MSL cores in order to see if any correlation with the noise outputs was apparent. Fig. 18 shows the rms velocity patterns on the front surface of the SSL and MSL CGO cores at 1.0 and 1.7 T. [Fig. 18(b) and (d) are duplicates of Fig. 11(a) and (c) and are added for clarity]. Interestingly, the vibration of the central limb is higher than that of the outer limb and yoke, but it is higher at both flux densities in the MSL-configured core although its noise output was lower as shown earlier. The average values of the rms velocity over the whole measured surface area at 1.0 T for the SSL and the MSL cores were 0.14 and 0.20 mm/s and the corresponding values at 1.7 T were 0.57 and 0.74 mm/s, respectively.

An interesting phenomenon, not clearly visible in Fig. 18. is the high vibration due to asymmetrical structure of the SSL design at 1.7 T. The same effect is present at 1.5 T.

The rms in-plane velocity distribution was also measured on the top and side surfaces of the two cores. The results for the CGO MSL core at 1.0 and 1.7 T are presented in Figs. 13 and 14. The distributions on the SSL core surfaces

TABLE IV
COMPARISON OF HARMONIC LEVELS OF OUT-OF-PLANE SURFACE rms VELOCITY [μm/s] AT POINTS IN THE MIDDLE LIMB (A/B/C), THE T-JOINT (D), AND THE CORNER JOINT (E) OF (a) MSL AND (b) SSL CGO CORES AT DIFFERENT FLUX DENSITIES. (BOLD FIGURES INDICATE HIGH VALUES COMPARED WITH THE OTHER CONFIGURATION)

(a)

f [Hz]	A/B/C (Centre limb)			D (T-joint)			E (Corners)		
	1.0 T	1.5 T	1.7 T	1.0 T	1.5 T	1.7 T	1.0 T	1.5 T	1.7 T
100	**313**	**747**	**1027**	**351**	1272	**1006**	348	276	957
200	11	36	**153**	25	**849**	1254	111	**378**	**1015**
300	4	10	**89**	32	**125**	682	18	334	**620**
400	3	19	**92**	10	349	294	11	96	165
500	2	17	**36**	2	110	**442**	13	142	205
600	1	7	59	3	68	**271**	8	**92**	**150**
Total (RMS)	**223**	**544**	**749**	187	492	673	**237**	**393**	**595**

(b)

f [Hz]	A/B/C (Centre limb)			D (T-joint)			E (Corners)		
	1.0 T	1.5 T	1.7 T	1.0 T	1.5 T	1.7 T	1.0 T	1.5 T	1.7 T
100	91	359	488	301	1258	464	**755**	**1301**	**1169**
200	13	**58**	89	**150**	690	**1475**	**283**	268	195
300	3	**23**	38	31	35	**890**	**54**	**353**	378
400	2	23	74	**22**	333	517	**18**	**134**	**328**
500	3	23	21	**24**	**170**	370	8	43	22
600	9	**35**	**153**	**16**	**114**	245	5	59	135
Total (RMS)	115	277	420	**213**	**809**	**1146**	106	326	479

were similar. The results for the CGO SSL core at 1.0 T approximately are 40 and 50 $\mu\varepsilon$ on the top and side surfaces, respectively, and at 1.7 T, they are approximately 100 and 100 $\mu\varepsilon$ on the top and side surfaces. The distribution of harmonics at fixed points in the central limb (A/B/C averaged), the T-joint (D), and the corner joint (E) in the two cores are compared in Table IV. The harmonics are shown in relative form to highlight the similarities and differences in the trends. Little information was lost since the levels in the SSL core were similar to those for the MSL core quantified in Table III.

The most significant findings that can be extracted from Table IV are: 1) the central limb of the MSL and SSL cores experience the highest 100 Hz vibration, which itself is higher in the MSL core at each flux density; 2) harmonics develop in the T-joints of both cores with increasing flux density, and at 1.7 T higher harmonics develop more prominently in the SSL core; 3) in the corner joint, at each flux density, the 100 Hz component is higher in the SSL core, but at 1.7 T, the 200 and 300 Hz components become significantly higher in the MSL core; and 4) the highest magnitudes of higher frequency harmonics occur in the T-joints of the two cores.

It can be seen that the first two harmonics have higher amplitude because of an effect of MS and that they are a source of noise. However, such low-frequency vibration is not picked up by the human ear. This is the reason why in some cases have higher vibration but lower noise.

Fig. 19 compares the harmonic spectrum of the rms velocity at points in the same three regions of the SSL and MSL cores

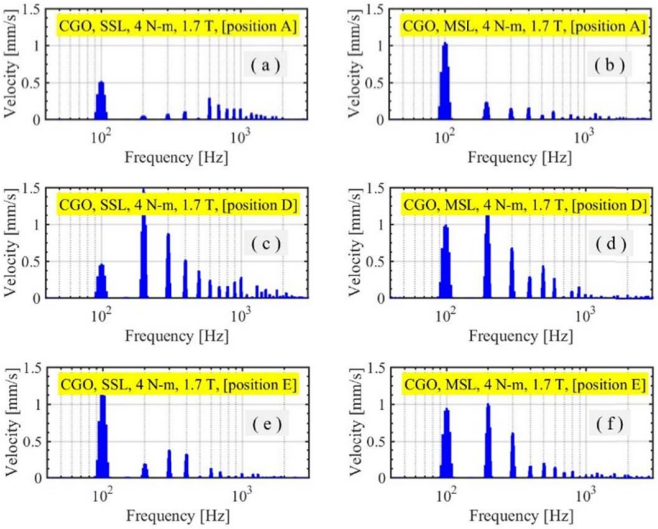

Fig. 19. Frequency distribution of out-of-plane rms harmonic components of vibration velocity (1.7 T, 4.0 N · m bolt torque). (a) Central limb, position A on SSL core. (b) Central limb, position A on MSL core. (c) Corner joint region, position D on SSL core. (d) Corner joint region, position D on MSL core. (e) T-joint region, position E on SSL core. (f) T-joint region, position E on MSL core.

at 1.7 T to highlight the trends shown in Tables I and IV. Considering the frequency distribution of the vibration component at 1.5 and 1.7 T, on the limb surface the frequency component at 100 Hz of the SSL is approximately half the amplitude of the MSL configuration (approximately 0.70 mm/s on MSL core and 0.35 mm/s on SSL core), while there are higher amplitudes of harmonic components near 1 kHz. This is the reason for higher A-weighted sound power level in the SSL core.

The surface velocity in the central limb of the SSL core has a higher harmonic content than that of the MSL core. The overall vibration in the central limb of the SSL core is lower than that of the MSL core but its impact on A-weighted noise would be higher. The trend in both corner joints is similar with very high harmonic levels (similar distribution in both cores suggests similar mechanisms), whereas in the T-joint, the MSL spectrum contains relatively higher harmonic levels.

E. Comparison of Single-Phase and Three-Phase Cores

Single- and three-phase cores of CGO were assembled with geometries shown in Fig. 5 using MSL joints and a clamping bolt torque of 4.0 N · m. They were magnetized at 1.5–1.7 T and the A-weighted sound power level was measured. The noise output from the single-phase core was around 2 dBA higher than that of the three-phase core at both flux densities. The cores are identical in size and construction apart from the central limb and T-joints of the three-phase core, which might be expected to contribute significantly to the noise.

The out-of-plane rms velocity was measured with a laser vibrometer averaged over surfaces of the two cores. The average vibration of the limb of the single-phase core was found to be four to five times less than that of the outer limbs of the three-phase core although its noise output was higher. However, the joint vibration in the single-phase core is considerably higher although magnetically the joints are identical.

The high vibration of the T-joint would be expected to produce a noise contribution not experienced by the single-phase core, but in spite of this, the three-phase core is quieter.

It may appear surprising that the noise of the single-phase core is higher and also that there does not seem to be any correlation between average surface vibration and acoustic noise. It can be partially explained by considering the time phase of the vibrations as discussed in Section IV-C, but the phenomenon needs more investigation.

V. Discussion and Conclusion

The most difficult hurdle in predicting the acoustic noise of three-phase transformer cores is quantifying the contribution of magnetostrictive and EM forces to the core vibration. The magnetostrictive forces can occur anywhere within the whole core volume, and although the EM forces are set up in the core joints, they also cause strain, hence potential vibration, throughout the whole core, so it is very difficult to isolate the effect of each on localized in-plane or out-of-plane vibration in laminations. It is possible that they interfere with each other, thus making the analysis even more complex.

The magnetostrictive forces can be minimized by use of low-MS GO material, hence reducing noise as illustrated in Table I, but the size of the reduction depends very much on the core joint configuration, with the less common SSL configuration showing a less predictable response to a low-MS material.

It is impossible to accurately estimate the contribution of magnetostrictive forces to core noise just from stress sensitivity of the type shown in Fig. 1. Incorporation of MS harmonics in the characterization seems essential just by noting the widespread occurrence of vibration harmonics in this study which are not linked in any obvious way to the fundamental (100 Hz) component, but no better means of quantifying the role of the harmonic has yet been verified.

The type of material had no influence on noise when SSL joints were used, except that at a very high flux density, the low-MS HGO core unexpectedly produced the highest noise. Since the EM-force-induced vibration should be mainly independent of the magnetic properties and flux density for a given geometry, this must be due to some magnetostrictive influence not quantified in the MS curves produced in the commonly used format as shown in Fig. 1. This is most possible since it is widely accepted that harmonics of MS are a major influence on A-weighted noise and they are not accounted for in any way in these characteristics.

Rotational MS is undoubtedly larger and more anisotropic than unidirectional MS at the same peak flux density [24], so it is often suggested as possibly being a significant source of noise in three-phase cores. However, the results shown in Section IV-A back up previous suggestions [32] that the degree to which it occurs in the transformer joints is much less than that is widely assumed because of the high anisotropy of GO; hence, it cannot be a direct cause of the high joint vibration strongly evident here.

There is no simple relationship between the magnitude and distribution of core surface displacement or velocity and acoustic noise. MS and forces between the ends of laminations in the joints cause in-plane forces expected to cause in-plane vibration throughout a core, but this is said to be only relevant on SSL cores [10]. The interlaminar forces at overlap regions in joints where high normal flux is present are a source of out-of-plane vibration which is partly responsible for the flapping of laminations at the joints. Noneffective clamping can lead to high corner vibration, but here changing the clamping pressure only caused noise changes within ± 0.7 dBA, which is within the limits of experimental accuracy.

The experimental results from Table I and Fig. 11 show that the rms velocity and displacement of out-of-plane vibration in all the cores tested were often more than five times higher than the in-plane values despite the fact that the origin is mainly the in-plane forces. This is related to the stiffness of the cores and needs further investigation. Previous investigation on a single-phase MSL core [9] found the ratio of front to top to side vibration velocity (nm/s) to be 157:140:6 at 1.6 T. The top surface velocity could be high because there is no restraining force from the T-joints, which increases the front face bending and introduces additional noise in the three-phase core.

The out-of-plane vibration of the central limb of the three-phase cores was consistently higher than that of the outer limbs. This is probably due to high strain in the T-joint, where the out-of-plane vibration is also high. The reason for the high T-joint vibration is unclear. Rotational MS might contribute to a small extent, but EM forces are the more likely cause even at low flux density. Fig. 15 shows how unsymmetrical in-plane strain can cause unrestrained MS extension of perhaps 10 μm which, if constrained by the core stiffness, is sufficient to cause the central limb bending. In-plane EM forces at the joints can also cause such unsymmetrical strain.

It is significant that the noise of the single-phase core is higher than that of the equivalent three-phase core with the same core cross-sectional area per phase and core window size, although the three-phase core is greater in volume and mass. This demonstrates the importance of the variation of the phase of the surface vibration throughout the core.

Table I shows that the 200 Hz component of surface out-of-plane-velocity is higher than the fundamental value in the T-joint and the corner joints at 1.5 and 1.7 T. If their A-weighted values are compared, the 100 Hz component is another 10 dBA less. The harmonics in the central limb vibration are far lower. From this, it can be inferred that the corresponding high 200 Hz and 300 Hz harmonics in the noise output shown in Fig. 10 are at least partly due to the corner vibrations. Previous measurements on a full-size commercial power transformer showed the dBA ratios of the first to fourth harmonics as approximately 1.0:0.86:0.96:0.82 [34]. The harmonic distribution in Fig. 10 is different, but they both illustrate the predominance of the low-frequency harmonics over the fundamental value which is commonly used as a reference. The measurements in [34] were made outside the transformer tank containing the core, so the harmonic distribution could be affected by mechanical resonance, etc.

The top and side surface vibration is mainly in the plane of the laminations and probably mainly produced by a different mechanism where the 100 Hz component is

dominant, possibly magnetostrictive in origin. However, the vibration harmonics on these surfaces are relatively lower than those on the front surface although the sound harmonics detected by the microphones facing these surfaces did contain higher harmonics whose distribution was somewhat similar to that of the total sound output.

Harmonics in the flux density across the butt joints might be a significant origin of vibration harmonics, but we are not aware of any reports quantifying this phenomenon. MS is probably the prime cause of the vibration harmonics. However, the MS of core materials is usually characterized in terms of their fundamental (100 Hz) component as in Fig. 1.

The MS components of the strips used in this investigation up to the tenth harmonic were measured independently [23]. Under zero stress and under tension, the peak-to-peak magnitudes were all less than 0.1 $\mu\varepsilon$, which was too close to the resolution of the measurements. At 1.7 T, 50 Hz magnetization, under a compressive stress of -10 MPa, the second and third harmonics of the MS in the CGO were 4.3 and 3.6 $\mu\varepsilon$, respectively, and the respective values for the HGO and LDR materials were 16% and 38%, and 32% and 70% less, respectively. This implies that the harmonic level of the MS of the LDR material is lowest, but it is based on one set of conditions which might not be representative of those in an actual core.

It has been shown how bending of the front face of the three-phase core can manifest itself as high vibration but this need not result in corresponding high noise. Harmonics of vibration and noise are not found to correlate but they dominate the frequency spectrum, so more effort is needed to find more suitable ways of characterizing MS to assess its impact on the noise of particular transformer core configurations. More knowledge of the actual stress distribution within cores is needed to help characterize MS in a more knowledge-based manner so that the effect on lamination vibration can be estimated more reliably.

The joints are undoubtedly the major source of vibration. It is claimed here that rotational MS might not be the dominant cause but only a full analytical study of the 3-D flux distribution and the associated MS can confirm its relevance. Reliable 3-D analysis would also form a foundation for a quantitative study of core joint deformation, which could lead to better understanding of the vibration mechanism needed to identify ways of substantially reducing core losses.

ACKNOWLEDGMENT

The investigation was carried out as part of a broader study of transformer noise. The authors would like to thank the project sponsors: ABB AB, AK Steel Corp, Alstom Grid, Brush Transformers Ltd, GC Holdings Belgium N.V., Cogent Power Ltd, Kolektor Etra Energetski Transformatorji d.o.o., Nuova Electrofer S.p.A., Koncar Distribution and Special Transformers Inc., Legnano Teknoelectric Company S.p.A., SGB Starksrom-Gerätebau GmbH, and ThyssenKrupp Electrical Steel GmbH for the financial support and technical input.

They would like to thank for the contribution of Mr. S. Tabrizi in carrying out and analyzing single strip magnetostriction measurements.

REFERENCES

[1] A. J. Moses and P. I. Anderson, "Effects of external stress on the magnetic properties of electrical steels," in *Proc. 5th Int. Conf. Magn. Metall. (WMM)*, Ghent, Belgium, Jun. 2012, pp. 87–100.

[2] E. Reiplinger, "Assessment of grain-oriented transformer sheets with respect to transformer noise," *J. Magn. Magn. Mater.*, vol. 21, no. 3, pp. 257–261, 1980.

[3] Z. Valkovic, "Effect of electrical steel grade on transformer core audible noise," *J. Magn. Magn. Mater.*, vol. 133, pp. 607–609, May 1994.

[4] M. Ishida, S. Okabe, T. Imamura, and M. Komatsubara, "Model transformer evaluation of high-permeability grain-oriented electrical steels," *J. Mater. Sci. Technol.*, vol. 16, no. 2, pp. 223–227, 2000.

[5] M. Ishida, S. Okabe, and K. Sato, "Analysis of noise emitted from three-phase stacked transformer model core," Kawasaki Steel, Japan, Tech. Rep. 39, 1998, pp. 29–35.

[6] J. Swaffield, "The causes and characteristics of transformer noise," *J. Inst. Electr. Eng. I, General*, vol. 89, no. 17, pp. 212–224, May 1942.

[7] A. Ilo, B. Weiser, T. Booth, and H. Pfützner, "Influence of geometric parameters on the magnetic properties of model transformer cores," *J. Magn. Magn. Mater.*, vol. 160, pp. 38–40, Jul. 1996.

[8] B. Weiser, A. Hasenzagl, T. Booth, and H. Pfützner, "Mechanisms of noise generation of model transformer cores," *J. Magn. Magn. Mater.*, vol. 160, pp. e207–e209, Jul. 1996.

[9] B. Weiser and H. Pfützner, "Relevance of magnetostatic forces for transformer core vibrations," *J. Phys. IV France*, vol. 8, pp. Pr2-591–Pr2-594, Jun. 1998.

[10] B. Weiser, H. Pfützner, and J. Anger, "Relevance of magnetostriction and forces for the generation of audible noise of transformer cores," *IEEE Trans. Magn.*, vol. 36, no. 5, pp. 3759–3777, Sep. 2000.

[11] R. Penin, J.-P. Lecointe, G. Parent, J.-F. Brudny, and T. Belgrand, "Grain-oriented steel rings for an experimental comparison of relative magnetostriction and Maxwell's forces effects," *IEEE Trans. Ind. Electron.*, vol. 61, no. 8, pp. 4374–4382, Aug. 2014.

[12] D. Snell, "Noise generated by model step lap core configurations of grain oriented electrical steel," *J. Magn. Magn. Mater.*, vol. 320, pp. e887–e890, Oct. 2008.

[13] M. Mizokami and Y. Kurosaki, "Variation of noise and magnetostriction associated with joint types of transformer core," *IEEJ Trans. Fundam. Mater.*, vol. 134, no. 5, pp. 334–339, 2014.

[14] Z. Valkovic, "Effects of transformer core design on noise level," *J. Phys. IV France*, vol. 8, no. PR2, pp. Pr2-603–Pr2-606, 1998.

[15] K. Jenkins and D. Snell, "Aspects of noise associated with GO electrical steels in transformer applications," Noise Mach., UK Magn. Soc. Seminar, Cardiff Univ., Cardiff, U.K., Seminar Rep. 2009, Feb. 2009.

[16] J. Anger and A. Daneryd, "Noise in power transformers- models for generation, transmission and propagation," Noise Mach., UK Magn. Soc. Seminar, Cardiff Univ., Cardiff, U.K., Seminar Rep. 2009, 2009.

[17] S. L. Foster and E. Reiplinger, "Charcteristics and control of transformer sound," *IEEE Trans. Power App. Syst.*, vol. PAS-100, no. 3, pp. 1072–1077, Mar. 1981.

[18] P. I. Anderson, A. J. Moses, and H. J. Stanbury, "Assessment of the stress sensitivity of magnetostriction in grain-oriented silicon steel," *IEEE Trans. Magn.*, vol. 43, no. 8, pp. 3467–3476, Aug. 2007.

[19] W. Gong *et al.*, "Magnetostriction and the influence of harmonics in flux density in electrical steel," *IEEE Trans. Magn.*, vol. 51, no. 11, Nov. 2015, Art. no. 6101404.

[20] P. Hamberger, "Low noise power transformers- more energy in large cities with less noise," Noise Mach., UK Magn. Soc. Seminar, Cardiff Univ., Cardiff, U.K., Seminar Rep. 2009, 2009, pp. 20–23.

[21] M. Mizokami, M. Yabumoto, and Y. Okazaki, "Vibration analysis of a 3-phase model transformer core," *IEEJ Trans. Fundam. Mater.*, vol. 119, no. 8, pp. 744–749, 1997.

[22] P. I. Anderson, A. J. Moses, and H. J. Stanbury, "An automated system for the measurement of magnetostriction in electrical steel sheet under applied stress," *J. Magn. Magn. Mater.*, vol. 215, pp. 714–716, Jun. 2000.

[23] S. Tabrizi, "Study of effective methods of characterisation of magnetostriction and its fundamental effect on transformer core noise," Ph.D. dissertation, School Eng., Cardiff Univ., Cardiff, U.K., Dec. 2013.

[24] M. Enokizono, S. Kano, and G. Shirakawa, "Measurement of arbitrary dynamic magnetostriction under alternating and rotating field," *IEEE Trans. Magn.*, vol. 31, no. 6, pp. 3409–3411, Nov. 1995.

[25] T. Phophongviwat, "Investigation of the influence of magnetostriction and magnetic forces on transformer core noise and vibration," Ph.D. dissertation, Cardiff Univ., Cardiff, U.K., Aug. 2013.

[26] D. Snell, "Measurement of noise associated with model transformer cores," *J. Magn. Magn. Mater.*, vol. 320, p. e535-e538, Oct. 2008.

[27] Z. Valkovic, "Investigations of core noise levels using a dry-type transformer model," *J. Magn. Magn. Mater.*, vol. 160, pp. 205–206, Jul. 1996.
[28] R. G. Budynas and K. J. Nisbett, *Shigley's Mechanical Engineering Design*, 9th ed. New York, NY, USA: McGraw-Hill, 2011.
[29] M. Jones, A. Moses, and J. Thompson, "Flux distribution and power loss in the mitered overlap joint in power transformer cores," *IEEE Trans. Magn.*, vol. 9, no. 2, pp. 114–121, Jun. 1973.
[30] F. Brailsford and J. M. Burgess, "Internal waveform distortion in silicon-iron laminations for magnetization at 50 c/s," *Proc. IEE C, Monographs*, vol. 108, no. 14, pp. 458–462, Sep. 1961.
[31] A. Moses and B. Thomas, "The spatial variation of localized power loss in two practical transformer T-joints," *IEEE Trans. Magn.*, vol. 9, no. 4, pp. 655–659, Dec. 1973.
[32] A. J. Moses, "The case for characterisation of rotational losses under pure rotational field conditions," *Preglad Elekrotechn.*, vol. 81, no. 12, pp. 1–4, 2005.
[33] L. Zhu, Q. Yang, and R. Yan, "Numerical analysis of vibration due to magnetostriction of three phase transformer core," in *Proc. 6th Int. Conf. Electromagn. Field Problems Appl. (ICEF)*, Jun. 2012, pp. 1–4.
[34] R. Girgis, J. Anger, and D. Chu, "The sound of silence: Designing and producing silent transformers," in *Proc. ABB Rev.*, 2008, pp. 47–51.
[35] G. Shilyashki *et al.*, "The impact of off-plane flux on losses and magnetostriction of transformer core steel," *IEEE Trans. Magn.*, vol. 50, no. 11, pp. 1–4, Nov. 2014.

Anthony John Moses (M'87–LM'15) was born in Newport, U.K. He received the B.Eng.Tech. degree in electrical engineering, the Ph.D. degree, and the D.Sc. degree for contribution to research into the properties and applications of soft magnetic materials from the University of Wales, Cardiff, U.K., in 1966, 1970, and 1990, respectively,

He was appointed as a Professor of Magnetics and the Director of the Wolfson Centre for Magnetics with Cardiff University, Cardiff, in 1992, where he was a Lecturer, Senior Lecturer, and Reader. Since 2012, he has been Emeritus Professor with Cardiff University. His current research interests include properties and applications of magnetic materials. He has authored over 500 publications and supervised over 100 post-graduate students in themes related to the production, characterization, and applications of magnetic materials.

Prof. Moses is a fellow of the Institute of Physics and the Institution of Engineering and Technology. He was a Chairman of the U.K. Magnetics Society and the International Organizing Committee of the Soft Magnetic Materials series of conferences. He is a member of organizing and editorial committees of several international conferences and journals.

Philip I. Anderson was born in U.K., in 1972. He received the B.Eng., M.Sc., and Ph.D. degrees from Cardiff University, Cardiff, U.K., in 2000.

He was with Cogent Power, Newport, U.K. He was a Researcher with the Wolfson Centre, Cardiff University, where he is currently Senior Lecturer of Magnetic Engineering. His current research interests include production, application, and characterization of soft magnetic materials.

Dr. Anderson is a Chartered Engineer and member of national and international standards committees on magnetic steels and alloys. He is currently a member of the international organizing committees of several major conference series, including Soft Magnetic Materials.

Teeraphon Phophongviwat was born in Kanchanaburi, Thailand. He received the B.Eng. and M.Eng. degrees in electrical engineering from the King Mongkut's Institute of Technology Ladkrabang (KMITL), Bangkok, Thailand, in 1999 and 2002, respectively, and the Ph.D. degree in electrical and electronic engineering from the Wolfson Centre for Magnetics, Cardiff University, Cardiff, U.K., in 2013.

He is currently with the Department of Electrical Engineering, Faculty of Engineering, KMITL. His current research interests include transformer, electrical machines, application and characterization of soft magnetic materials, finite element, and optimization techniques.